

Supplementary

SiO₂/GST/SiO₂ sandwich structure

The cross-sectional TEM image of Fig. S1(a) shows the sample structure of the GST film with a thermally-grown SiO₂ substrate and capping materials after annealing at 500°C. Both interfaces of GST/SiO₂ were well maintained and defined without loss of the initial layered structure. To confirm the macroscopic interdiffusion and/or mass transportation along the vertical direction of the sample structure, the atomic distribution was analyzed by EDS. Figure S1(b) shows the variations in atomic concentrations with depth, which indicates the concentration of the GST layer and corroborates the target composition, indicating that there is no macroscopic mass transportation.

Effect of the final temperatures and ramping rates on crystallization behavior

Figure S2(a) shows the non-polarized Raman spectra of GST as a function of the final temperatures (T_f) with a ramping rate of 1140K. The Raman mode of 120 and 150 cm⁻¹ clearly shows that the GST remains as the amorphous phase at 250 °C due to a shift in the crystallization temperature to a higher temperature. The onset of formation of the hexagonal phase at 550 °C, compared with that near 300 °C with the conventional ramping rate of below 10 K/min, also helps to describe the T_c shift induced by the fast ramping rate. Moreover, evolution of the Raman mode shows that the cubic phase of GST is initiated and partially formed at 350 °C, which is consistent with the XRD results shown in Fig. S2(b). The partial presence of the cubic phase indicates that grain growth is effectively suppressed, and crystallization is under the control of nucleation dominant kinetics. According to Orava et al., the kinetic coefficient for crystal growth of GST shows a significant non-Arrhenius temperature dependence.¹ Likewise, GST in the supercooled liquid state is very fragile, comparable to

fragile liquids such as those reported in oxide and organic systems.² The behavior of a fragile liquid is strongly dependent on the temperature. The atomic mobility characterized by viscosity is low near the glass transition temperature, while viscosity markedly decreases with increasing temperature. Additionally, if the GST film is surrounded by dielectric materials (SiO_2 in this paper), the viscosity of the amorphous matrix effectively increases due to the constraint of adjacent dielectric materials.^{3, 4} Therefore, the partial formation of the cubic phase in the amorphous matrix can be described by the higher effective activation energy required for viscous flow at relatively lower temperatures. As T_f increases, the amorphous matrix is more fragile and has lower viscosity, and crystallization proceeds against lower effective activation energy. The Raman mode for the octahedral configuration of the cubic phase is more enhanced at a T_f of 450 °C. Therefore, the stress relaxation process for crystallization takes place at lower viscosity, and the response for the relaxation process such as structural deformation and phase separation is more detectable at higher T_f , especially by spectroscopic measurement. Likewise, this phenomenon is also observed in the ramping rate dependence, as shown in Fig. S3 (a) and (b). As the ramping rate increases, T_c also rises, as observed in previous studies.^{3, 5} A high ramping rate facilitates the investigation of crystallization kinetics at higher temperatures. Besides, the stress induced by crystallization itself can be easily relaxed due to the low viscosity of the remaining amorphous matrix. The variations in Raman mode and XRD clearly show the presence of a separated phase at the highest ramping rate, which is consistent with the results of T_f dependence. As a result, there is no detectable distortion of Raman and XRD spectra at low T_f and ramping rates, but high T_f and the highest ramping rate are able to provide the opportunity to acquire an enhanced relaxed state.

References

1. J. Orava, A. L. Greer, B. Gholipour, D. W. Hewak and C. E. Smith, *Nat Mater*, 2012, **11**, 279-283.
2. M. D. Ediger, P. Harrowell and L. Yu, *J Chem Phys*, 2008, **128**, 034709.
3. J. Orava, A. L. Greer, B. Gholipour, D. W. Hewak and C. E. Smith, *Appl Phys Lett*, 2012, **101**, 091906.
4. R. Pandian, B. J. Kooi, J. T. M. De Hosson and A. Pauza, *J Appl Phys*, 2006, **100**, 123511.
5. Y. Choi, M. Jung and Y. K. Lee, *Electrochim Solid St*, 2009, **12**, F17-F19.

Tables

Table S1. Stress tensor of the initial and the relaxed heterostructure

| | <i>XX</i> | <i>YY</i> | <i>ZZ</i> | <i>XY</i> | <i>YZ</i> | <i>ZX</i> |
|-------------------------|-----------|-----------|-----------|-----------|-----------|-----------|
| Initial heterostructure | 0.420 | 1.609 | 0.728 | -0.179 | -0.055 | 0.176 |
| Relaxed heterostructure | -0.072 | 0.748 | -0.573 | 0.010 | -0.012 | 0.146 |

Figure captions

Figure S1. (a) Low magnification cross-sectional TEM image of the GST film annealed at 500°C. (b) The atomic concentration of constituents along the red line of the TEM image by EDS.

Figure S2. Effect of final temperature and a fast ramping rate of 1140 K/min on crystallization behavior. (a) Changes in the non-polarized Raman spectra of GST with variation in the final temperature. The cubic phase is partially formed at 350 oC, which indicates the suppression of crystal growth due to low viscosity. As Tf increases, the hexagonal phase is formed through the cubic phase (as the parent phase of the hexagonal phase). (b) X-ray diffraction patterns of GST as a function of the final temperature and a ramping rate of 1140 K/min. The diffraction plane of the separated phase clearly appears at 500 oC, where the peaks denoted by * are the corresponding peaks of the separated phase.

Figure S3. Effect of fast ramping rates on crystallization behavior. (a) Changes in the slope occur in high frequency mode as ramping rates increase at a final temperature of 500 °C, due to the onset of phase separation. (b) X-ray diffraction pattern of GST with various ramping rates.

The highest ramping rate facilitates the formation of the separated phase denoted by *.

Figure S4. The partial radial distribution function (PRDF) of (a) the Ge-Te and (b) Sb-Te bonding with tensile stress.

Figure S5. The heterostructure composed of the junction between the (111) surface of the cubic and the (0001) surface of the hexagonal structure, which initially includes intrinsic monovacancy at the interface. The lattice parameter fits an average value from both the systems, and the mismatch of the lattice parameters are $\pm 0.24\%$ (a), $\pm 1.29\%$ (b) and $\pm 0.02\%$ (γ).

Figure S6. The total radial distribution function averaged from (a) the cubic, (b) interface, and (c) hexagonal parts.

Figure S1

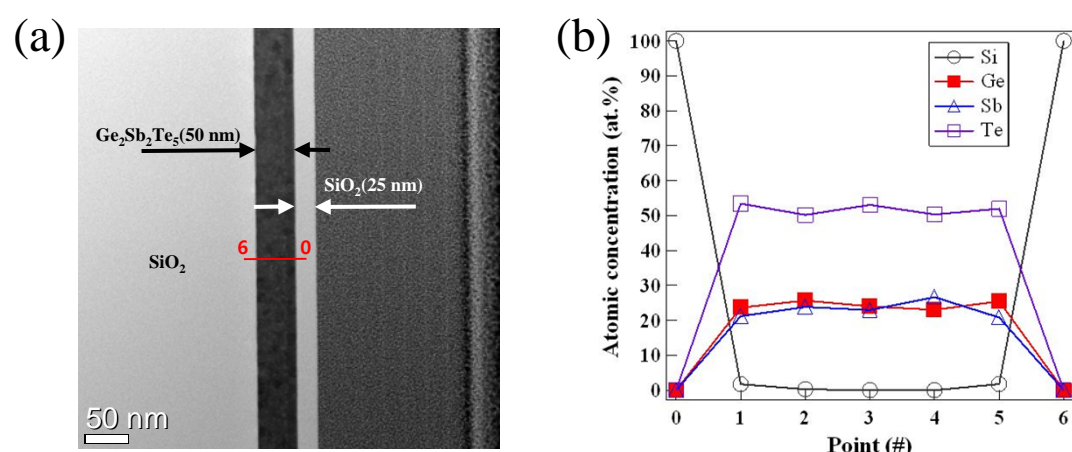


Figure S1 Park *et al.*

Figure S2

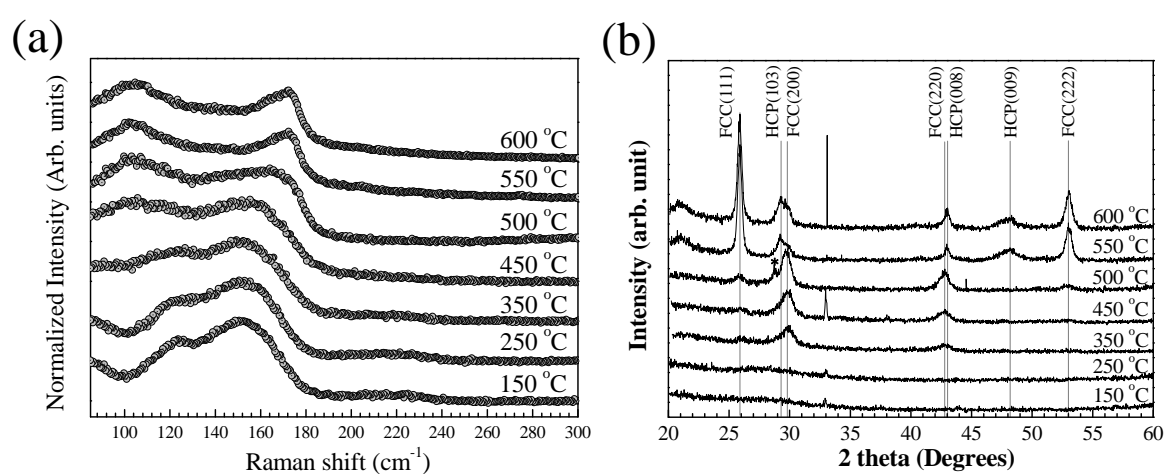


Figure S2 Park *et al.*

Figure S3

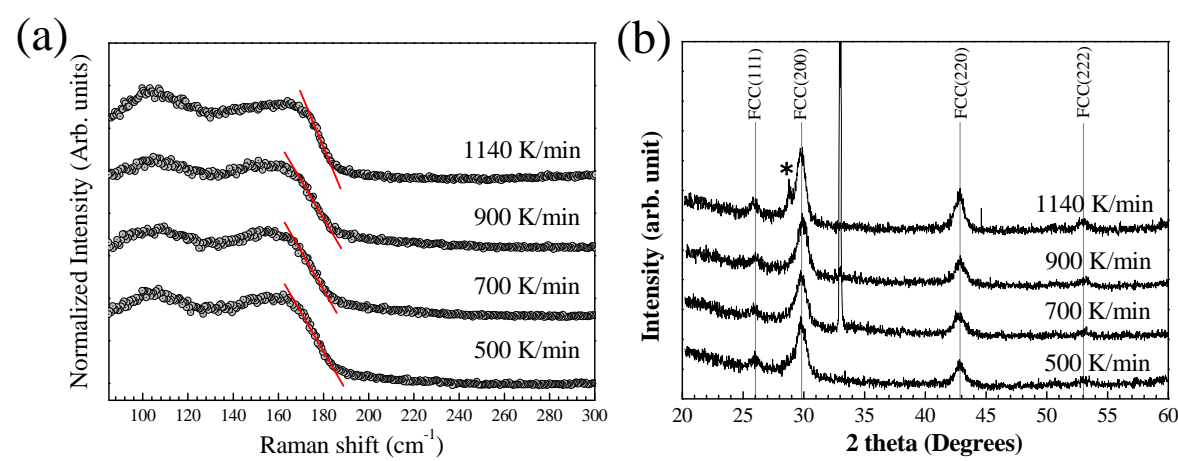


Figure S3 Park *et al.*

Figure S4

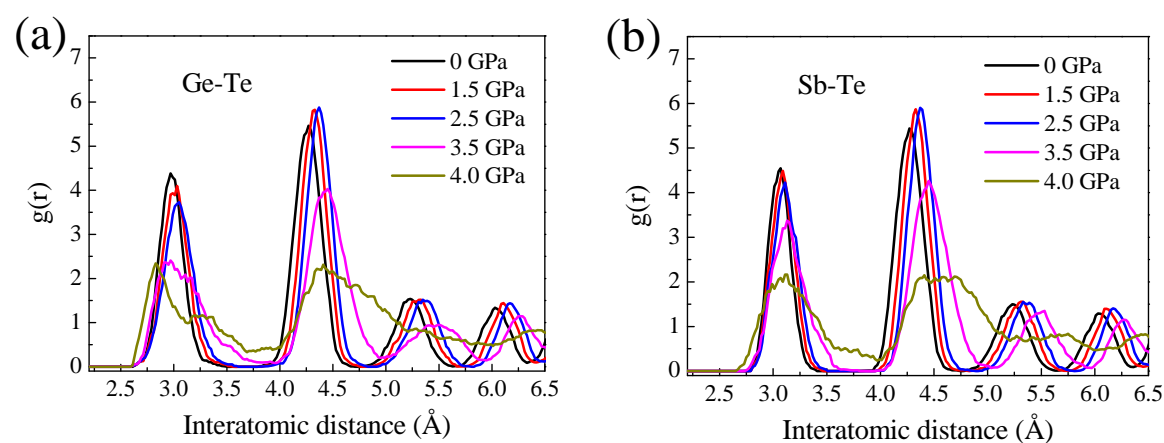


Figure S4 Park *et al.*

Figure S5

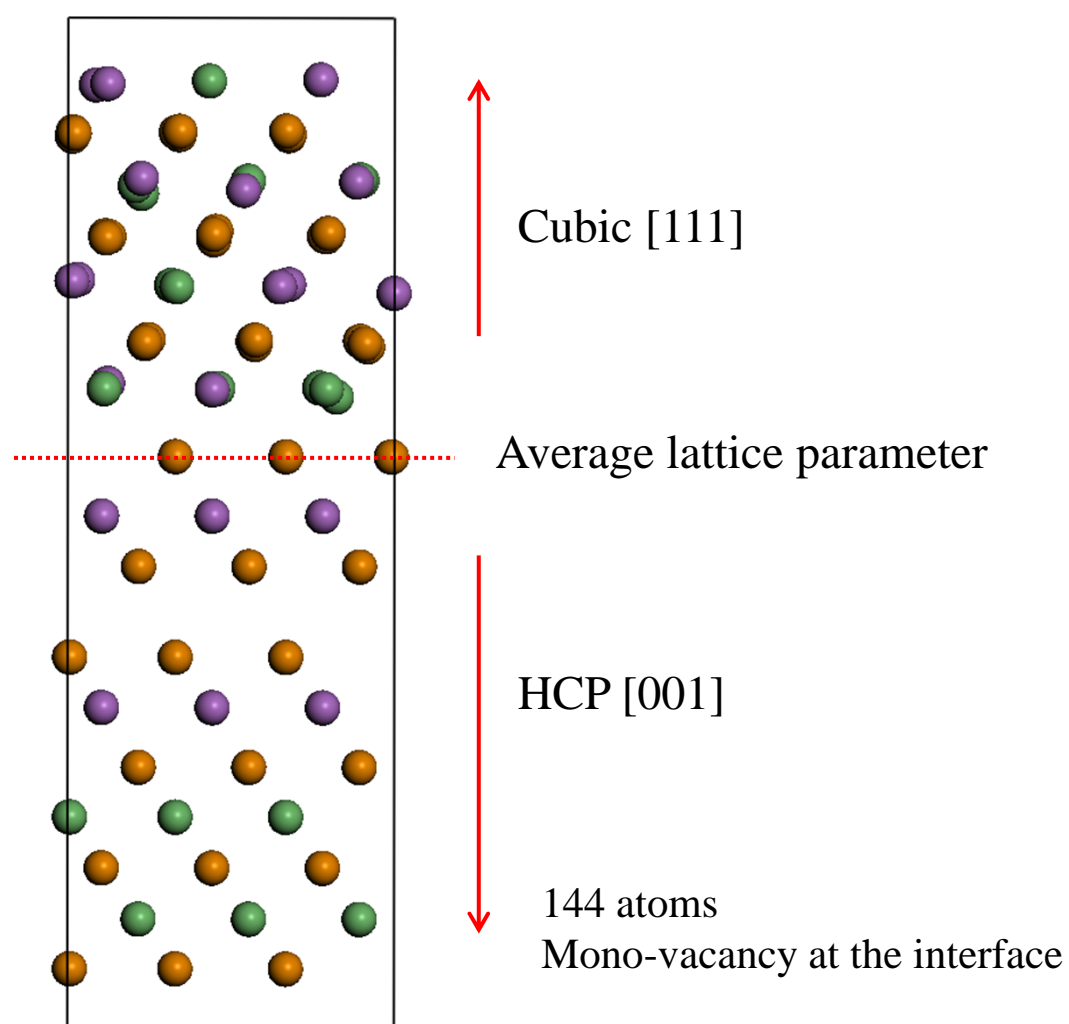


Figure S5 Park *et al.*

Figure S6

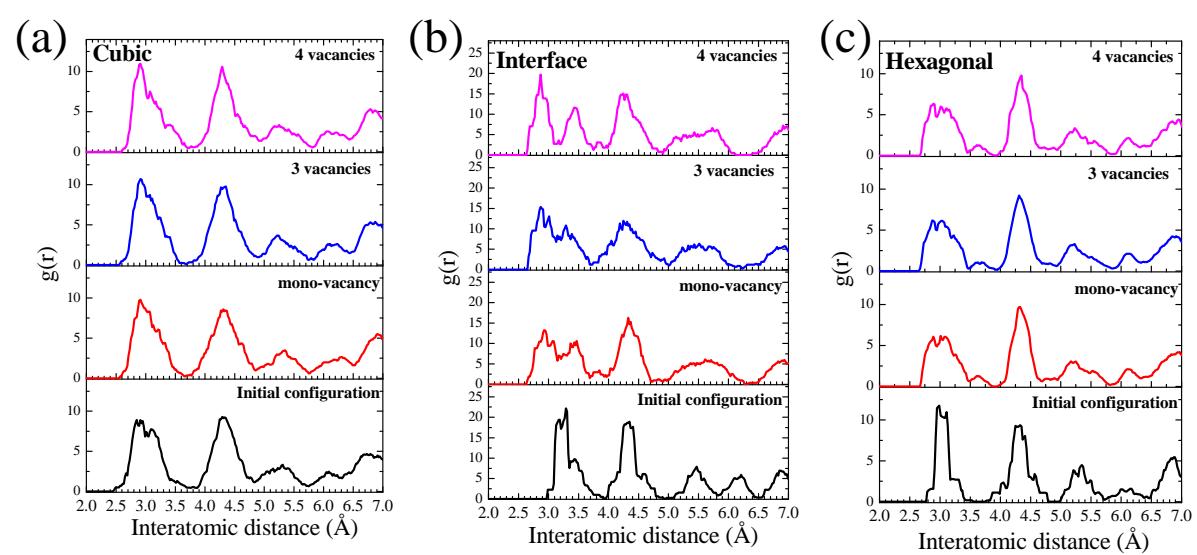


Figure S6 Park *et al.*